Bent-Beam Strain Sensors

Yogesh B. Gianchandani, *Member, IEEE,* and Khalil Najafi, *Member, IEEE*

***Abstract*— We examine a new class of sensitive and compact passive strain sensors that utilize a pair of narrow bent beams with an apex at their mid-points. The narrow beams amplify and transform deformations caused by residual stress into opposing displacements of the apices, where vernier scales are positioned to quantify the deformation. An analytical method to correlate vernier readings to residual stress is outlined, and its results are corroborated by finite-element modeling. It is shown that tensile and compressive residual stress levels below 10 MPa, corresponding to strains below 6×10^{-5}, can be measured in a 1.5-μm-thick layer of polysilicon using a pair of beams that are 2 μm wide, 200 μm long, and bent 0.05 radians (2.86°) to the long axis of the device. Experimental data is presented from bent-beam strain sensors that were fabricated from boron-doped single crystal silicon using the dissolved wafer process and from polycrystalline silicon using surface micromachining. Measurements from these devices agree well with those obtained by other methods. [125]**

I. Introduction

An IMPORTANT aspect of characterizing the mechanical properties of materials for microstructures involves the measurement of residual stress of thin films. Many different techniques to perform these measurements have been developed in past years. One approach uses measurements of changes in wafer curvature to calculate average film stress. Commercial instruments are available that measure wafer curvature using lasers and then compute the stress. Another approach relies on the deformation produced by external loading in specially designed structures to calculate material properties like Young's modulus and residual stress in a spatially localized manner. Examples of this are the load-deflection of composite membranes [1], electrostatic pull-in of bridges [2], and frequency measurements of resonant microstructures [3], [4]. A third approach uses strain sensors designed to operate passively. These are basically undercut structures that deform measurably under the residual stress of the material. Passive strain sensors that have been developed in the past include bridges and rings that buckle under compressive and tensile stresses, respectively [5], T-shaped structures with wide, long center beams, and thinner, deformable cross beams that provide a measure of the deformation either directly [6] or by tilting a long cantilever [7], and bridges with an intermediate lateral displacement that rotate a long pointer when deformed [8], [9].

Passive strain sensors are attractive because they can provide quantitative readout from an observation of the deformation under a microscope. With the exception of the buckling beams and bridges, however, all of the devices that have been developed in the past are very large (1–4 mm) in at least one dimension. This means that they occupy a large area and also limit spatial resolution. Furthermore, some of these devices employ long cantilevers to multiply the strain displacement [7]–[9]. Long cantilevers are susceptible to out-of-plane deformation, caused by a nonuniform distribution of stress through the cross section of the device, making the readout more difficult and less reliable. Buckling rings and bridges are smaller than other passive strain sensors that have been developed in the past, but they require the use of many copies to achieve adequate range and resolution. Also, the precision of measurements made by buckling devices is reduced by slight imperfections in the material and geometry of the device, which make buckling a continuous function of residual stress rather than a threshold function [10]. Many of the devices developed in the past also have the additional disadvantage of only being able to measure either compressive or tensile strain, but not both. This paper presents a new class of strain sensors that use bent beams to achieve high resolution and sensitivity for tensile and compressive materials while offering significant advantages in size and resistance to unwanted out-of-plane deformation [11], [12]. A simple analytical model has been developed to correlate the measured deformation to the residual stress, and it has been verified by finite-element modeling. Bent-beam devices have been fabricated and used to measure residual stress in polysilicon thin films and in heavily boron doped silicon. These measurements have been compared with results obtained with a commercial tool that calculates residual stress from the change in curvature of an unpatterned wafer.

II. Device Structure and Modeling

An SEM micrograph of a fabricated bent-beam strain sensor is shown in Fig. 1. The device is basically a 400-μm-long bridge clamped at both ends. Half this undercut length is 100 μm wide, whereas the other half is comprised of two 4-μm-wide V-shaped beams bent towards each other at their midpoints, making an angle of 0.1 radians with the long axis of the bridge. A vernier scale is located at this point to measure deformation caused by the residual stress. The vernier has a nominal resolution of 0.2 μm and range of ± 1.0 μm. (The pitch of the tines is governed by processing constraints, and this particular design was chosen as a compromise between range and resolution for a reasonable vernier length.) A simple model for the behavior of the strain sensor is provided in Fig. 2. The elasticity of the structural material is modeled by springs k1, k2, and k3 for the single wide and two narrow

Manuscript received July 26, 1994; revised October 26, 1995. Subject Editor, A. P. Pisano. This work was supported by NSF grant ECS-8915215 and ARPA contract 92-2340.

The authors are with the Center for Integrated Sensors and Circuits, University of Michigan, Ann Arbor, MI 48109-2122 USA.

Publisher Item Identifier S 1057-7157(96)01466-7.

1057–7157/96$05.00 © 1996 IEEE

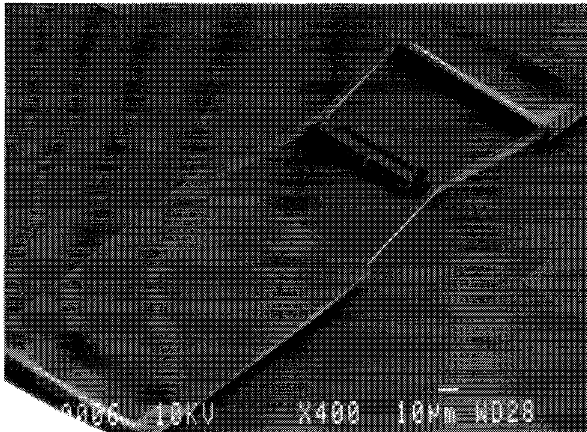

Fig. 1. A scanning electron micrograph of a (type B) bent-beam strain sensor fabricated using a bulk silicon dissolved wafer process.

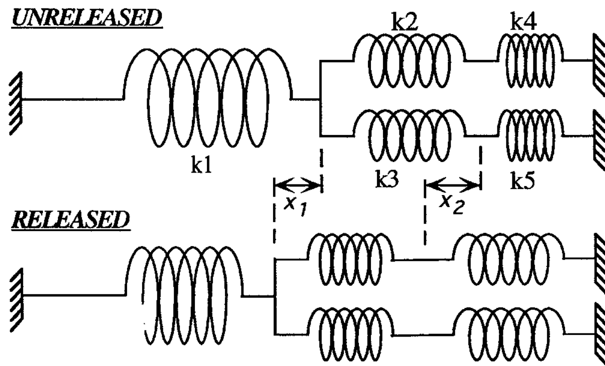

Fig. 2. A simple model for the response of a (type B) strain sensor to tensile material. The springs k1, k2, and k3 model stretching of the material, whereas k4 and k5 model bending of the narrow beams. The vernier quantifies the extension in k4 and k5, which is then correlated to the stress.

regions, respectively. The elasticity due to bending of the two narrow beams is modeled by k4 and k5. Fig. 2 qualitatively shows the state of each spring in the unreleased and released states for tensile material. The former corresponds to the point in fabrication just after the structural material has been deposited and patterned, and the latter corresponds to the finished structure after the sacrificial material is removed. In the unreleased state, the material may have residual stress, but the structure is not measurably deformed. When the device is freed and responds to this stress, the wide portion of the bridge relaxes, causing a deformation in the bent beam springs that is a combination of bending and stretching. The transverse displacement of the apex is about 10× more than the longitudinal displacement x_2 caused by the bending of the narrow beams (Fig. 2). This amplification of the motion is due to the angle of the beams: their motion is like that of parallelogram actuators [13]. Some of the net amplification is lost because of the elasticity of the material itself. If the beams are at a very shallow angle the elasticity of the material contributes more to the extension of the beams than does their bending ($x_1 > x_2$). Since the apices move towards each other, the apparent vernier displacement is further amplified by two. The readout of the vernier provides a quantitative measure of the strain.

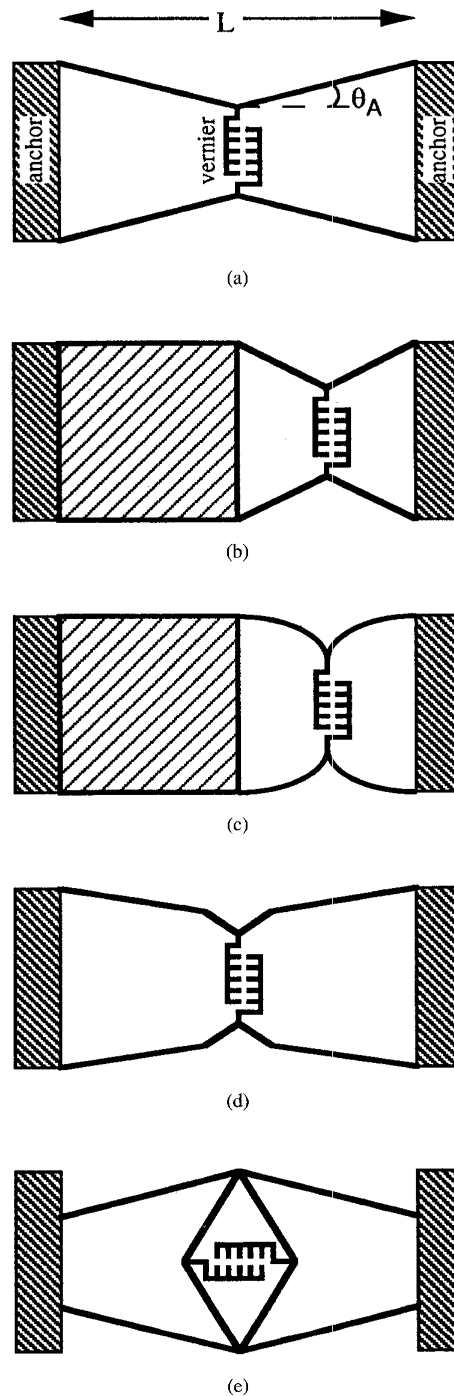

Fig. 3. Various topologies of bent-beam strain sensors with vernier scales to quantify the deformation.

Topologies for a variety of passive bent-beam strain sensors are illustrated in Fig. 3. The basic design, shown as type A, uses a pair of V-shaped beams bent at their mid-points. Type B is the kind of device shown in Fig. 1, with a wide section

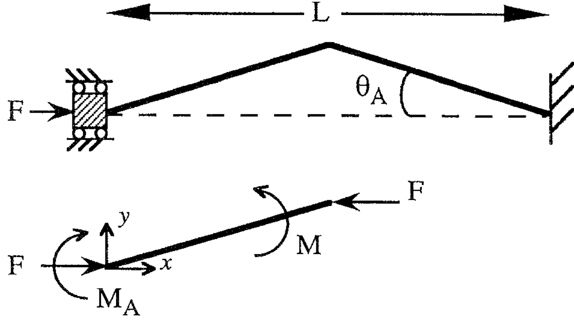

Fig. 4. Forces acting on a bent beam in a strain sensor. F is the axial force used to model the effects of the stress, M_A is the moment from the supporting anchor, and M is the moment in the beam at an arbitrary value of x.

in one half of its bridge length and a pair of V-shaped beams in the other half. Type C is similar, except that the beams are curved and meet the wide section at right angles. The trade-off associated with topologies A, B, and C will be explored in later sections. Types D and E are examples of more complex designs that can be constructed by combining beams at different angles and by nesting the basic structure, with potential benefits in range and sensitivity.

A. Analytical Modeling

The bent-beam strain sensors can be modeled analytically using simple beam theory. Consider a single bent beam constrained as shown in Fig. 4, with one end fixed and the other end guided along the x axis. F is the force necessary to keep the beam in its post-release deformed shape. It is related first to the y axis displacement of the apex, which corresponds to one half of the vernier readout, and then to the x axis displacement of the guided end, which represents the strain in the bridge. This strain is related to the residual stress in the material by the Young's modulus of the material, which must be known *a priori*. In this way, the residual stress associated with any given value of the vernier readout can be determined. For single crystal silicon, in which Young's modulus is anisotropic [14], the value used is that for the long axis of the bent beam strain sensors. For all the devices described in this paper, the angle made by the bent beams with this axis is $<6^\circ$. For all the devices that were fabricated, the long axis was aligned to the (001) crystal orientation on the substrate wafer.

The governing equation and the boundary conditions for the left half of the bent beam in Fig. 4 are

$$\begin{aligned} EI\frac{\partial^2 y}{\partial x^2} &= M = M_A - Fy; \\ y|_{x=0} &= 0; \\ \left.\frac{\partial y}{\partial x}\right|_{x=0} &= \left.\frac{\partial y}{\partial x}\right|_{x=L/2} = \tan\theta_A \end{aligned} \tag{1}$$

where E and I are, respectively, the Young's modulus and the moment of inertia for the beam. All the other symbols are defined in Fig. 4. When F is tensile, the solution of these equations is given by

$$y = \frac{\tan\theta_A}{k}\left[\tanh\frac{kL}{4}(1-\cosh kx) + \sinh kx\right]$$

where

$$\begin{aligned} k &= \sqrt{F/EI}; \\ y_{\text{apex}} &= y|_{x=L/2} = 2\frac{\tan\theta_A}{k}\tanh\frac{kL}{4}. \end{aligned} \tag{2a}$$

When F is compressive the solution is

$$\begin{aligned} y &= \frac{\tan\theta_A}{k}\left[\tan\frac{kL}{4}(1-\cos kx) + \sin kx\right] \\ y_{\text{apex}} &= y|_{x=L/2} = 2\frac{\tan\theta_A}{k}\tan\frac{kL}{4}. \end{aligned} \tag{2b}$$

The vernier reading corresponding to an applied force F is given by $2\Delta y = 2(y_{\text{apex}} - y_o)$, where y_o is the location of the apex in the unreleased structure.

For an arbitrary axial load F, the apparent shortening of the bent beams can be obtained by using the formula [15]

$$\frac{L'}{2} = -\frac{1}{2}\int_0^{L/2}\left(\frac{\partial y}{\partial x}\right)^2 dx \tag{3}$$

where L' is the difference between the actual length of the beam and its projected length along the x axis. Then, using (2) and (3)

$$\begin{aligned} L' = \frac{(\tan\theta_A)^2}{4k}[&2H + kL - kLH^2 + \sinh kL \\ &- 2H\cosh kL + H^2\cosh kL] \end{aligned}$$

in tension and

$$\begin{aligned} L' = \frac{(\tan\theta_A)^2}{4k}[&2G + kL + kLG^2 + \sin kL \\ &- 2G\cos kL - G^2\sin kL] \end{aligned}$$

in compression, where $G = \tan(kL/4)$ and $H = \tanh(kL/4)$. The V-shaped beams bend such that L' increases and decreases with compressive and tensile loads, respectively. The change in L', however, does not account for elastic stretching of the material. The net displacement along the x axis is obtained by adding the bending and stretching contributions of the V-shaped beams, and this value can be used to calculate residual stress in the material. For the type A strain sensor

$$\sigma = E\varepsilon = \frac{E}{L}(\Delta L' + \frac{FL}{Ewh}) \tag{4}$$

where $\Delta L'$ is the change in L' caused by the applied force F, and w and h are the width and height of the bent beams. The link between stress and the vernier readout is, therefore, established using the force F.

Fig. 5 shows the responses for type A structures with three different values of θ_A using $L = 200$ μm, $w = 2$ μm, and $h = 1.5$ μm. The material is assumed to be polycrystalline silicon, with $E = 160$ GPa. The analysis shows that for $\theta_A = 0.05$ rad, the value of stress that corresponds to a vernier reading of 0.2 μm is 9.18 MPa in tension and 9.30 MPa in compression, and that the responses are linear over a range of hundreds of MPa. These values of sensitivity and range

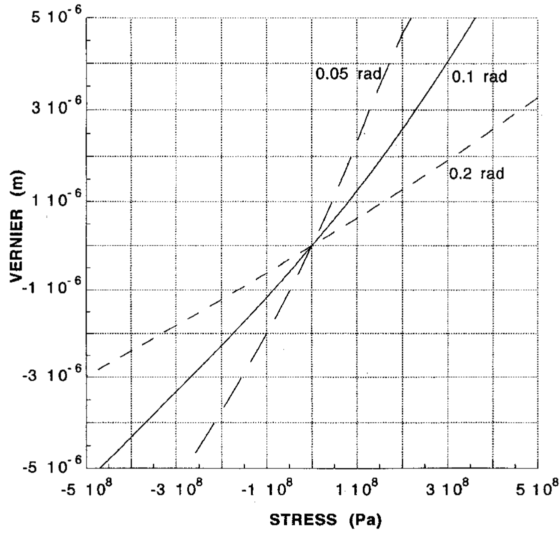

Fig. 5. Analytically obtained responses for type A bent-beam strain sensors with $L = 200$ μm, $w = 2$ μm, $h = 1.5$ μm, $E = 160$ GPa, and three different values of θ_A.

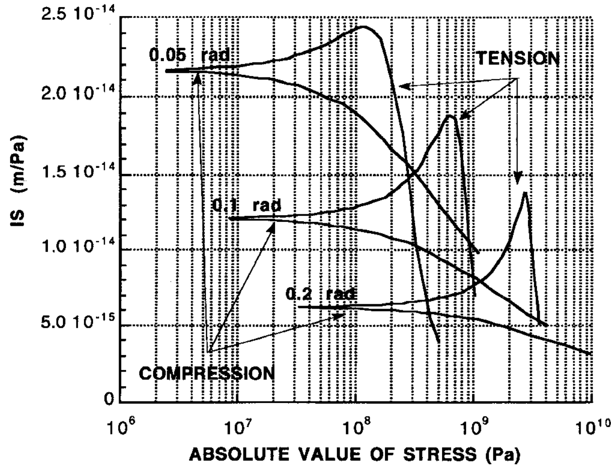

Fig. 6. Variation of incremental sensitivity (IS) with stress for the three type A structures defined in Fig. 5. IS is the change in the vernier reading for a small increment in stress.

compare very favorably with passive strain sensors that have been developed in the past, particularly if the size of the device is taken into account.

The curves in Fig. 5 show that the response of the strain sensors tends toward nonlinearity at high stress levels. In order to gain further insight into how this happens, it helps to examine the incremental sensitivity of the strain sensors. Incremental sensitivity (IS) is defined as the change in the vernier for a small increment in the stress. Fig. 6 shows the variation of IS with stress for the same devices that were analyzed in Fig. 5. It is clear that for low stress levels in both tension and compression, the device with the smallest θ_A is the most sensitive. This is because the y displacement of the apex is greater for smaller values of θ_A. It is for the same reason that IS initially improves with stress in tensile material: the

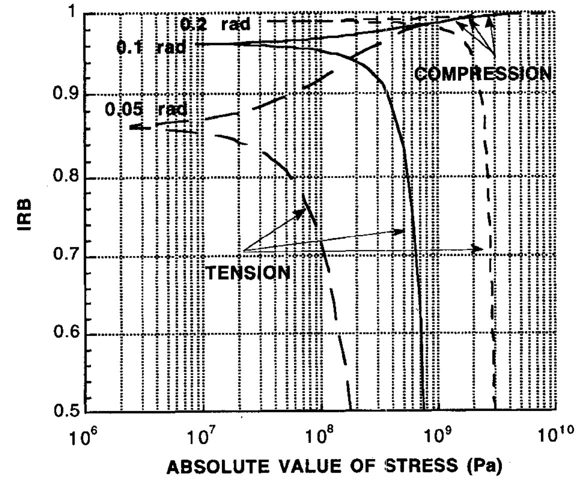

Fig. 7. Variation of the incremental ratio of bending (IRB) with stress for the three type A structures defined in Fig. 5. IRB is the fractional contribution of beam bending to the incremental strain.

effective θ_A is reduced as ends of the beam are pulled apart. Beyond a point, however, the contribution from the stretching of the material exceeds that from the bending of the V beams and leads to a sharp decline in IS. This effect can be clearly observed in Fig. 7, which shows the variation with stress of the incremental ratio of bending (IRB). IRB can be defined as the change in $\Delta L'/[\Delta L' + (FL/Ewh)]$ caused by a small change in stress. Fig. 7 shows that for the device with $\theta_A = 0.05$ rad. the incremental deformation caused by tensile stress levels above a few hundred MPa is increasingly dominated by the stretching of the material, causing a rapid decline in IS. Fig. 7 also shows that devices with lower values of θ_A have lower IRB. For compressive materials, the effective θ_A increases as the stress increases, thereby improving the IRB but degrading the IS. The proper choice of θ_A for a bent-beam strain sensor, therefore, depends on the range and resolution desired.

The analysis above has focused primarily on type A bent-beam strain sensors. It is informative to compare this topology with some of its alternatives. Fig. 8 shows how IS varies with stress for type A, B, and C designs. All three designs have $L = 400$ μm, $w = 4$ μm, $h = 6$ μm, and $\theta_A = 0.1$ rad., and are assumed to be fabricated from $p+$ silicon, with $E = 175$ GPa. The type C strain sensor has the best low-stress sensitivity of the three, whereas the type B sensor sustains a uniform response over the widest range of stress. Note that in analyzing type B and C strain sensors, the basic approach is the same as that used above for type A devices. The only important differences are that since the bent beams are half the length of the bridge, and since the wide section of the bridge sustains a negligible fraction of the residual stress, (3) and (4) change to

$$L' = -\frac{1}{2}\int_0^{L/2}\left(\frac{\partial y}{\partial x}\right)^2 dx$$

$$\sigma = E\varepsilon = \frac{E}{L}\left(\Delta L' + \frac{FL}{2Ewh}\right).$$

(Formulas for the response of type C beams can be found in [16] and are similar to those developed by this analysis.) It is interesting that reducing the length of the bent beams to half the undercut length of the bridge does not significantly decrease the low-stress IS.

An important performance limit that must be evaluated for the bent beam strain sensors is the critical value of compressive stress for which the bridges will buckle. For the type A device (2b) indicates that $y_{\text{apex}} \to \infty$ as $kL \to 2\pi$, which means that the critical compressive force for lateral buckling is

$$F_{cr} = \frac{EI4\pi^2}{L^2}.$$

This is identical to the formula for the critical compressive force of a straight beam of length L. The critical force can be translated to a value of compressive stress in the material that will cause the bridge to buckle upon release, which is undesirable in this type of sensor. For the type C device analyzed in Fig. 8 the thickness of each bent beam is greater than its width, so lateral buckling dominates (although it is not a threshold phenomenon), and the critical compressive stress is greater than 1 GPa. For the type A devices described in Figs. 5–7, vertical buckling dominates and the critical compressive stress is greater than 2 GPa. Herein lies another advantage of the bent-beam strain sensors: the devices can be made so small that their buckling stresses are higher than the residual stresses found in most microstructure materials.

B. Finite-Element Modeling

Finite-element modeling (FEM) has been performed using ANSYS to confirm some of the analytical results described above. Stress was introduced in the model by the standard technique of applying a uniform temperature change

$$\sigma = \Delta T E \alpha$$

where ΔT = temperature change and α = the thermal expansion coefficient. Fig. 9 compares the relative apex displacements obtained analytically with those obtained by FEM for a type B device of dimensions as described in Fig. 8. The difference between the FEM and analytically obtained displacements is less than 5% between −300 and +100 MPa and rises to 13% at +300 MPa. This demonstrates that for the device considered, the analytical approach is valid over the entire range of stress in which its IS curves (Fig. 8) remain relatively flat. The FEM also confirms that in the released structure the wide region of the bridge sustains negligible stress, as was assumed in the analytical model.

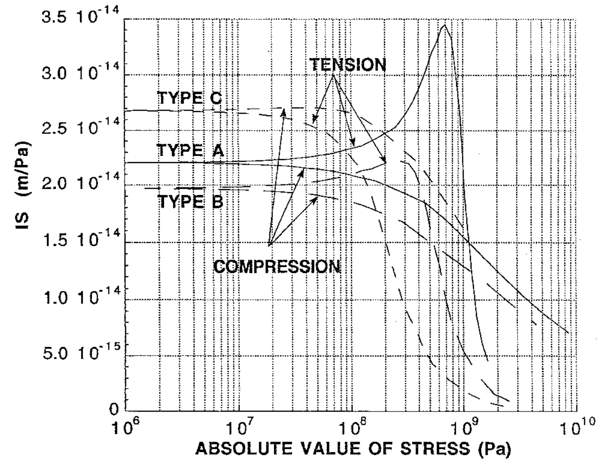

Fig. 8. Analytical comparison of type A, B, and C strain sensors with $L = 400$ μm, $w = 4$ μm, $h = 6$ μm, $E = 175$ GPa, and $\theta_A = 0.1$ rad.

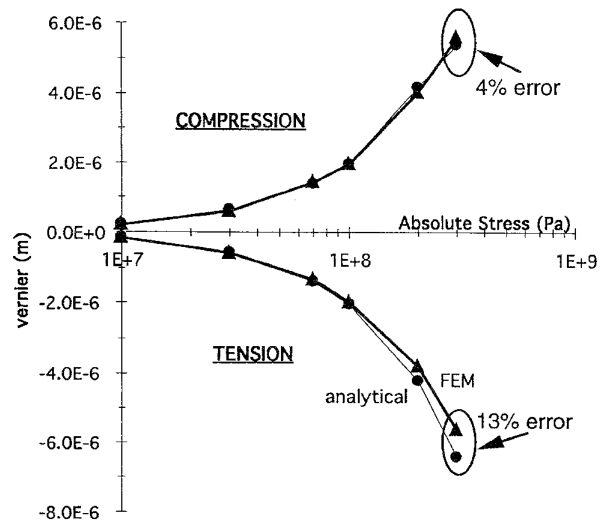

Fig. 9. Comparison of the vernier displacements obtained analytically and by FEM for a type B device with dimensions as described in Fig. 8.

III. Experimental Results & Discussion

Type A strain sensors with $L = 200$ μm, $w = 2;$ μm, $h = 1.5$ μm, and $\theta_A = 0.1$ rad. were fabricated by surface micromachining of polysilicon. LPCVD polysilicon was deposited at 625°C on about 1 μm of oxide thermally grown on (100) silicon substrates. The wafers were then subjected to different combinations of doping and annealing. The dopant was phosphorous, and it was diffused at 950°C for 60 min. The annealing was performed in nitrogen at 1050°C for 60 min. The polysilicon was then patterned, and the sacrificial oxide under it was etched away. Some unpatterned control wafers were also fabricated to measure film stress from the change in wafer curvature using a commercial Flexus 2-300 machine. The oxide and polysilicon were removed from the backs of the control wafers before measurement. Table I shows the Flexus readings, the strain sensor deflections, and the corresponding values of stress obtained by the analytical method for a variety of processing conditions. The Flexus and strain sensor results were consistent with each other. As expected, the undoped, unannealed polysilicon was found to be in high compressive stress. Fig. 10(a) shows that for this material the deflection of the bent-beam strain sensor was beyond the 1 μm measurement range of the vernier incorporated into the design.

TABLE I
MEASUREMENTS OF TYPE A STRAIN SENSORS WITH $L = 200\ \mu$m, $w = 2\ \mu$m, AND $h = 1.5\ \mu$m, FABRICATED FROM POLYSILICON WITH OPTIONAL PHOSPHOROUS DOPING AND NITROGEN ANNEALING. INTRINSIC STRESS OBTAINED ANALYTICALLY USING $E = 160$ GPa IS COMPARED TO FLEXUS MEASUREMENTS, WHICH ARE DERIVED FROM THE CHANGE IN WAFER CURVATURE

doped	annealed	vernier (μm)	Analytical stress (MPa)	Flexus stress (MPa)
Y	Y	-0.4 ±0.1	-33.5 ±8	-26.6
Y	N	-0.2 ±0.1	-16.7 ±8	-17.4
N	Y	-0.1 ±0.1	-8.3 ±8	–
N	N	-2.4 ±0.2	-211 ±18	-231

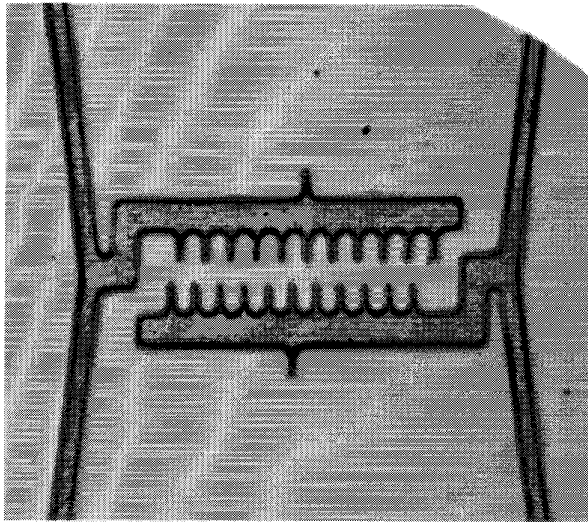

(a)

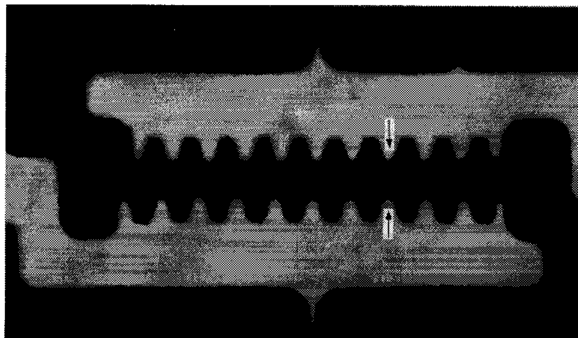

(b)

Fig. 10. (a) An optical micrograph of about 2.4-μm compressive vernier deflection in a polysilicon bent-beam strain sensor. The vernier is 56 μm long. (b) A tensile vernier deflection of about 0.4 μm in p^+ silicon.

The reading was taken with a calibrated microscope. Doping or annealing the polysilicon caused a significant reduction in the intrinsic stress.

Type B strain sensors, as shown in Fig. 1, were fabricated from boron-doped bulk silicon by the dissolved wafer processes described in [4] and [17]. Vernier readings from different fabrication runs and the corresponding values of residual stress obtained analytically are listed in Table II, and

TABLE II
MEASUREMENTS OF 400-μ-m LONG TYPE B STRUCTURES MADE FROM p^+ Si DURING DIFFERENT FABRICATION RUNS OF THE DISSOLVED WAFER PROCESS. RESIDUAL STRESS WAS OBTAINED BY THE ANALYTICAL METHOD USING E =175 GPa. OTHER MEASUREMENT TECHNIQUES HAVE INDICATED RESIDUAL STRESSES OF 15–40 MPa FOR THIS TYPE OF MATERIAL

sample no.	sample name	vernier (μm)	width (μm)	thickness (μm)	residual stress (MPa)
1	401g2	0.4 ±0.1	2.5	5.55	18 ±5
2	402a2	0.4 ±0.1	2.8	6.75	19 ±5
3	402b	0.4 ±0.1	3.6	7.28	20 ±5
4	401b	0.5 ±0.1	2.8	6.53	23 ±5
5	401f2	0.6 ±0.1	1.6	5.40	27 ±5
6	401d2	0.6 ±0.1	2.4	6.27	27 ±5
7	401f1	0.6 ±0.1	3.2	6.21	29 ±5
8	401a	0.6 ±0.1	4.0	5.41	30 ±5

a sample photograph of the vernier displacement is shown in Fig. 10(b). The residual stress ranged from 18–30 MPa (tensile). In comparison, past measurements at this laboratory using the pull-in voltage technique [2] and the resonant frequency technique [4] have yielded tensile residual stresses of 18.3 MPa and 18.5± 4 MPa, respectively.

There are several potential sources of error in the strain sensor measurements. For devices with beams as thick and narrow as those in Table II, one source of error is nonuniformity in beam width along the x and z axes. A second possible source of error is the out-of-plane deformation of the device, which may result from stress gradients in the material. This is particularly true of the verniers, which are cantilevered, and provides a reason to keep them short. A sample calculation helps to quantify the rough magnitude of this error. For the devices reported here, the vernier scales are about 56 μm long and have a minimum resolution of 0.2 μm. This means that the out of plane deformation, if approximated as a straight line, would have to be in excess of 3 μm at the tip in order to cause an apparent displacement of 0.1 μm on each side of the vernier and thereby register as a minimum reading on the scale. Such a large out-of-plane displacement can be detected under a microscope and was not seen in any of the devices reported here. A third possible source of error is the compliance of the supporting anchors of the strain sensor. The error in calculating the maximum deflection due to a point load in the center of a bridge can exceed 10% when its length is less than about 100 μm, but reduces below 5% when the length is greater than about 200 μm [18]. For the device dimensions described in this paper, the compliance of the anchors is not a significant source of error.

It is worth noting that although the small size of bent-beam sensors greatly helps to reduce their susceptibility to stiction, it does not make them immune to this problem. When the devices are thick and suspended several microns above the substrate, such as those in Table II, they do not clamp to the substrate. When both the structural material and the sacrificial layer underneath it are thin, as for those in Table I, clamping can and does occur. Although the sensors are able to fully respond to the residual stresses before they clamp to the substrate upon removal from the wet sacrificial etch, this must be recognized as another potential source of error in the readings.

IV. Conclusion

A new class of sensitive and compact passive strain sensors has been presented. The designs use pairs of bent beams to amplify deformations caused by residual stress in the structural material. The beams are designed to cause complementary motion in a vernier scale, thereby doubling the sensitivity of the device. Various designs have been presented and evaluated. It has been shown, for example, that a structure which is only 200 μm long can be used to sense tensile or compressive stress below 10 MPa, with its linear response range extending to more than 100 MPa. A simple analytical technique, based on the deflection of the beams and the elastic extension of the material, has been described for modeling the strain sensors. It has been verified by finite-element modeling and by experimental methods. Bent beam strain sensors have been fabricated from boron-doped silicon and phosphorous-doped polysilicon and have yielded results consistent with other measurement techniques.

Acknowledgment

The authors gratefully acknowledge helpful discussions with Dr. S. Crary, Dr. G. K. Ananthasuresh, and L. Saggere regarding modeling issues and the assistance of C. C. Huang in fabricating some of the samples used in this study.

References

[1] O. Tabata, K. Kawahata, S. Sugiyama, and I. Igarashi, "Mechanical property measurements of thin films using load-deflection of composite rectangular membrane," in *Proc. IEEE Workshop on Microelectromechanical Systems (MEMS '89)*, 1989, pp. 152–156.

[2] K. Najafi and K. Suzuki, "A novel technique and structure for the measurement of intrinsic stress and Young's modulus of thin films," in *Proc. IEEE Workshop on Microelectromechanical Systems (MEMS '89)*, 1989, pp. 96–97.

[3] L.M. Zhang, D. Uttamchandani, and B. Culshaw, "Measurement of the mechanical properties of silicon microresonators," *Sensors and Actuators A*, 29, pp. 79–84, 1991.

[4] Y. Gianchandani and K. Najafi, "A bulk silicon dissolved wafer process for microelectromechanical devices," *J. Microelectromechanical Syst.*, vol. 1, no. 2, pp. 77–85, June 1992.

[5] H. Guckel, D. Burns, C. Rutigliano, E. Lovell, and B. Choi, "Diagnostic microstructures for the measurement of intrinsic strain in thin films," *J. Micromech. Microeng.*, vol. 2, pp. 86–95, 1992.

[6] M. Mehregany, R. Howe, and S. Senturia, "Novel microstructures for the in situ measurement of the mechanical properties of thin films," *J. Appl. Phys.* vol. 62, no. 9, pp. 3579–3584, 1 Nov. 1987.

[7] L. Lin, R. Howe, and A. Pisano, "A passive in situ micro strain gauge," in *Proc. IEEE Workshop Microelectromechanical Syst. (MEMS '93)*, 1993, pp. 201–206.

[8] L. B. Wilner, "Strain and strain relief in highly doped silicon," in *Tech. Dig. IEEE Solid-State Sensor & Actuator Workshop (Hilton Head '92)*, June 1992, pp. 76–77.

[9] J. F. L. Goosen, B. P. van Drieenhuisen, P. J. French, and R. F. Wolffenbuttel, "Stress measurement structures for micromachined sensors," in *Proc. Int. Conf. on Solid-State Sensors and Actuators (Transducers '93)*, July 1993, pp. 783–786.

[10] W. Fang and J. A. Wickert, "Post-buckling of micromachined beams," in *Proc. IEEE Workshop Microelectromechanical Syst. (MEMS '94)*, Jan. 1994, pp. 182–187.

[11] Y. B. Gianchandani and K. Najafi, "A compact, passive strain sensor with a bent beam deformation multiplier and a complementary motion vernier," in *Tech. Dig. Solid-State Sensor & Actuator Workshop (Hilton Head '94)*, June 1994, pp. 116–118.

[12] P. M. Zavracky, G. G. Adams, and P. D. Aquilino, "Strain analysis of silicon-on-insulator films produced by zone melting recrystallization," *J. Microelectromechanical Syst.*, vol. 4, no. 1, pp. 42–48, Mar. 1995.

[13] N. Takeshima, K. Gabriel, M. Ozaki, J. Takahashi, H. Horiguchi, and H. Fujita, "Electrostatic parallelogram actuators," in *Proc. Int. Conf. Solid-State Sensors and Actuators (Transducers '91)*, July 1991, pp. 63–66.

[14] J. J. Wortman and R. A. Evans, "Young's modulus, shear modulus, and Poisson's ratio in silicon and germanium," *J. Applied Phys.* vol. 36, no. 1, pp. 153–156, Jan. 1965.

[15] R. J. Roark and W. C. Young, *Formulas for Stress and Strain.* New York: McGraw-Hill, 1975, p. 98.

[16] ——, *Formulas for Stress and Strain.* New York: McGraw-Hill, 1975, pp. 162–168.

[17] Y. Gianchandani, K. Najafi, and B. Orr, "Silicon micromachined thermal profilers," in *Tech. Dig., Int. Electron Devices Meet. (IEDM)*, Washington, D.C., Dec. 1994, pp. 191–194.

[18] Q. Meng, M. Mehregany, and R. L. Mullen, "Theoretical modeling of microfabricated beams with elastically restrained supports," *J. Microelectromechanical Syst.*, vol. 2, no. 3, pp. 128–137, Sept. 1993.

Yogesh B. Gianchandani (S'83–M'85–S'90–M'94) received the B.S.E.E. degree from the University of California, Irvine, in 1984, the M.S.E.E. degree from the University of California, Los Angeles, in 1986, and the Ph.D. degree in electrical engineering from the University of Michigan, Ann Arbor, in 1994.

His work at Xerox Corporation from 1985 to 1988 and at Microchip Technology from 1988 to 1989 focused on the design of integrated circuits. He is presently involved in all aspects of design, fabrication, and packaging of micromachined sensor and actuator systems, both as a Research Fellow at the University of Michigan, Ann Arbor, and as a private consultant. He has contributed to a variety of micromachined devices, including accelerometers, resonant microactuators, strain sensors, thermal profilers, and implantable biomedical transducers.

Dr. Gianchandani is a member of Tau Beta Pi and Eta Kappa Nu.

Khalil Najafi (S'84–M'86) was born in 1958. He received the B.S.E.E. degree in 1980 and the M.S.E.E. degree in 1981, both from the University of Michigan, Ann Arbor. He received the Ph.D. degree in electrical engineering from the University of Michigan in 1986.

From 1986 to 1988 he was employed as a Research Fellow, from 1988 to 1990 as an Assistant Research Scientist, from 1990 to 1993 as an Assistant Professor, and since September 1993 as an Associate Professor in the Department of Electrical Engineering and Computer Science, University of Michigan, Ann Arbor. His research interests include the development, design, fabrication, and testing of: solid-state integrated sensors and microactuators; analog and digital integrated circuits; implantable microtelemetry systems and transducers for biomedical applications; technologies and structures for microelectromechanical systems and microstructures; and packaging techniques for implantable transducers.

Dr. Najafi was awarded a National Science Foundation Young Investigator Award from 1992–1997, was the recipient of the Beatrice Winner Award for Editorial Excellence at the 1986 International Solid-State Circuits Conference, and he was awarded the Paul Rappaport Award for co-authoring the Best Paper published in the IEEE Transactions on Electron Devices. He received the University of Michigan's Henry Russel Award for outstanding teaching and scholarship in 1995. He is an Associate Editor for the *Journal of Micromechanics and Microengineering*.